European Journal of Radiology 118 (2019) 51–57

Contents lists available at ScienceDirect

European Journal of Radiology

journal homepage: www.elsevier.com/locate/ejrad

Research article

# Can DCE-MRI reduce the number of PI-RADS v.2 false positive findings? Role of quantitative pharmacokinetic parameters in prostate lesions characterization

Giulia Cristel[a,*], Antonio Esposito[a,b], Anna Damascelli[a], Alberto Briganti[b,c], Alessandro Ambrosi[b], Giorgio Brembilla[a,b], Lisa Brunetti[a,b], Sofia Antunes[a], Massimo Freschi[d], Francesco Montorsi[b,c], Alessandro Del Maschio[a,b], Francesco De Cobelli[a,b]

[a] Department of Radiology, Experimental Imaging Center, San Raffaele Scientific Institute, via Olgettina 60, 20132 Milan, Italy
[b] Vita Salute San Raffaele University, via Olgettina 60, 20132 Milan, Italy
[c] Department of Urology, San Raffaele Scientific Institute, via Olgettina 60, 20132 Milan, Italy
[d] Department of Pathology, San Raffaele Scientific Institute, via Olgettina 60, 20132 Milan, Italy

ARTICLE INFO

*Keywords:*
Magnetic resonance imaging
Prostatic neoplasms
Diagnosis
Perfusion imaging

ABSTRACT

*Purpose:* To test the potential impact of pharmacokinetic parameters, derived from DCE-MRI analysis, on the diagnostic performance of PI-RADSv.2 classification in prostate lesions characterization.

*Method:* Among patients who underwent multiparametric prostate MRI (mpMRI) (January 2016-March 2018) followed by histological evaluation (targeted biopsies/prostatectomy), 103 men were retrospectively selected. For each patient the index lesion was identified and pharmacokinetic parameters (Ktrans, Kep, Ve, Vp) were assessed. MRI diagnostic performance in the detection of significant tumors [Gleason Score (GS) ≥ 7] was assessed, considering PI-RADS ≥ 3 as positive.

*Results:* GS ≥ 7 (n = 59) showed higher Ktrans ($p < 0.01$) and Kep ($p = 0.01$) compared to GS < 7. At ROC curve analysis, a Ktrans cut-off of 191 × $10^{-3}$/min was identified to predict the presence of GS ≥ 7 (AUC:0.75; sensitivity:95%; specificity:61%). Sensitivity and PPV of mpMRI using PI-RADSv.2 were 98% and 61%. Reclassifying PI-RADS ≥ 3 lesions according to Ktrans cut-off, 22 false positives were shifted to true negatives with 3 false negative findings; PPV raised to 79%. Appling Ktrans cut-off to PI-RADS 3 lesions of peripheral zone (n = 18), 12 true negatives, 4 true positives, 2 false positives were identified.

*Conclusions:* Despite its high sensitivity prostate mpMRI generates many false positive cases: Ktrans in addition to PIRADS v.2 seems to improve MRI-PPV and may help in avoiding redundant biopsies.

## 1. Introduction

Prostate cancer (PCa) is the most frequently diagnosed tumor and the second and third-most common cause of cancer death among men in US and Europe, respectively [1,2].

Multiparametric magnetic resonance (mpMRI), which includes T2-weighted (T2W), diffusion weighted (DWI), and Dynamic Contrast-Enhanced (DCE) imaging, has become an essential tool in patients work-up, providing reliable information for detection, localization, characterization and staging of PCa [3,4].

Thanks to its high sensitivity and negative predictive value, mpMRI has recently been proposed as a triage-test for target biopsy, in men with elevated serum PSA (Prostate Specific Antigen) [5,6]. On the other hand, due to its relatively low specificity and positive predictive value mpMRI still produces a consistent number of false positive results and therefore unnecessary biopsies [7–10].

PI-RADS (Prostate imaging reporting and data system) version 2, is one of the most utilized reporting system for prostate mpMRI [3]. It consists in a 5-point scale classification that summarizes the levels of risk of clinically significant prostate cancer based on mpMRI findings,

*Abbreviations:* PCa, prostate cancer; mpMRI, multi-parametric magnetic resonance imaging; T2W, T2-weighted; DWI, diffusion weighted imaging; DCE, dynamic contrast-enhanced; PI-RADS, prostate imaging reporting and data system; PSA, prostate specific antigen; PK, pharmacokinetic; ADC, apparent diffusion coefficient; GS, gleason score; AIF, arterial input function; ROI, region of interest; PZ, peripheral zone; TZ, transition zone; $K^{trans}$, transfer constant; $K_{ep}$, rate constant; Ve, extravascular extracellular volume fraction; Vp, plasma volume fraction

* Corresponding author at: Department of Radiology, San Raffaele Scientific Institute, Vita-Salute San Raffaele University, via Olgettina 60, 20132 Milano, Italy.
*E-mail address:* cristel.giulia@hsr.it (G. Cristel).

https://doi.org/10.1016/j.ejrad.2019.07.002
Received 18 February 2019; Received in revised form 16 June 2019; Accepted 1 July 2019

**Table 1**
Imaging protocol details.

| Parameter | T2 TSE axial | T2 TSE sagittal | T2 TSE coronal | DWI (b: 50, 800, 1600) | DCE |
|---|---|---|---|---|---|
| *TR (ms)* | 4824 | 4370 | 2991 | 4376 | 3.7 |
| *TE (ms)* | 120 | 120 | 120 | 80 | 1.83 |
| *FOV (mm)* | 180 × 180 | 180 × 180 | 180 × 180 | 180 × 180 | 180 × 180 |
| *Matrix* | 512 × 512 | 512 × 512 | 512 × 512 | 144 × 144 | 280 × 280 |
| *Thickness (mm)* | 3 | 3 | 3 | 3 | 3 |
| *Gap (mm)* | 0.3 | 0.3 | 0.3 | 0.3 | 0 |
| *Flip angle (°)* | 90 | 90 | 90 | 90 | 5,8,12,15 |
| *Acquisition time* | 4min 6s | 3min 25s | 2min 8s | 5min 19s | 3min 20s |

*Note-* TE = echo time; TR = repetition time; TSE = turbo spin-echo; DWI = diffusion-weighted imaging, DCE = dynamic contrast enhanced, FOV = field of view.

considering T2W, DWI and DCE sequences [11]. Compared to PI-RADS v1, in this latest version the role of DCE has become secondary to DWI and T2W images and is based on qualitative and subjective assessment of focal enhancement in a suspicious area. Like in many other tumors the enhancement pattern of PCa is usually different from the surrounding normal tissue, with tumor showing an earlier and more pronounced uptake of contrast medium. This behavior is thought to be related to the deregulation of angiogenic pathway in PCa, that leads to an increased release of angiogenic factors. As result the number of vessels increase and these newly formed vessels have weaker and more permeable walls [12–14]. Quantitative parameters obtained from pharmacokinetic (PK) models applied to DCE-MRI are known to provide information related to capillary permeability, blood fraction and interstitial space volume. These parameters have demonstrated superior performance to differentiate between cancerous and normal prostatic tissue, compared to qualitative or semi-quantitative enhancement analysis [15,16].

In this study we explored the potential role of PK parameters in the implementation of mpMRI diagnostic performance based on PI-RADS v2, aiming to reduce the number of false positive findings and increase MRI positive predictive value.

The secondary endpoint was to evaluate the impact of PK parameters in the management of intermediate risk lesions (PI-RADS 3), in which the presence of clinically significance cancer is equivocal, that still represents a challenging issue of mpMRI [17].

## 2. Material and methods

### 2.1. Patient population

Our Institutional Review Board approved this retrospective study. We used archived patient data from our institutional database. All men undergoing mpMRI of the prostate at our hospital (and consequently all patients enrolled in this analysis) provided written informed consent for having their data collected for research purposes before the scan. From our Data Base of 666 prostate mpMRI, acquired between January 2016 (time of incorporation of a new DCE sequence into our prostate MR imaging protocol) and March 2018, we retrospectively selected patients with available corresponding histological specimen obtained through targeted biopsies or prostatectomy, performed at our Institution after MRI examination. We retrieved 112 men and excluded those with poor quality imaging (n = 5) and with MR performed without endorectal coil (n = 4). The final population consisted of 103 patients (mean age: 64; range: 45–83); the mean PSA value was 8 ng/ml (range: 3,7–69).

Prostate specimens were processed according to the Stanford protocol [18] and analyzed by a dedicated uro-pathologist with 20 years of experience.

### 2.2. MRI protocol

All patients underwent a 1.5-T mpMRI study (Achieva and Achieva dStream, Philips Medical Systems, Best, Netherlands) with a balloon-covered expandable endorectal coil (BPX-15™, Bayer Medical Care, Indianola, PA, USA) paired with a phased array 5 or 32-channel surface coil, depending on the scanner. Gastrointestinal peristalsis was suppressed by intramuscular administration of 20 mg of scopolamine-butylbromide (Buscopan, Boehringer Ingelheim, Ingelheim, Germany) in all men. The imaging protocol consisted of multiplanar turbo spin-echo T2-weighted images, echo-planar DWI (*b* values: 50-800-1600s/mm$^2$, with automatic ADC maps generation based on a pixel-by-pixel elaboration using both two and three b values), multiple flip angle T1-weighted images for T1 mapping and 3D fast field-echo DCE MRI (temporal resolution 4.1 s) acquired during an intravenous bolus injection of 0.1 mmol/kg of gadobutrol (Gadovist, Bayer Schering Pharma, Germany), administered at 3.5 mL/s with an automatic injector (Spectris® MR Injector System, Medrad®, Indianola, PA, USA), followed by 20 mL saline at the same injection rate.

Imaging protocol details are listed in Table 1.

### 2.3. MRI image analysis

All images were reported according to PI-RADS v2 guidelines [3]. Two radiologists (** and *** with 10 and 7 years of experience on prostate mpMRI interpretation, respectively), blinded to clinical and histopathological information, independently reviewed and analyzed all the images, selecting for each patient the index lesion. The index lesion was identified as the lesion with the highest PI-RADS score. If two or more lesions with same PI-RADS score were present, the largest one was considered for the analysis. Of note, histopathological data were available for all the target areas included in our study.

Images were analyzed with a commercial available permeability software (IntelliSpace Portal v.7, Philips Healthcare, Best, The Netherlands) approved by United States Food and Drug administration. Pharmacokinetic parameters were calculated from DCE images using the modified Toft model and a population-based arterial input function (AIF) as previously reported [19–21]. For each patient both radiologists manually drew three regions of interest (ROIs) on the subtracted image sets from the DCE-MRI, using T2-weighted images or ADC map for the morphologic reference. The first ROI outlined the index lesion within the peripheral (PZ) or transition (TZ) zone. The second and the third ROIs were placed in normal PZ and TZ areas.

For each resulting ROI the following perfusion parameters were calculated: transfer constant ($K^{trans}$), rate constant ($K_{ep}$), extravascular extracellular volume fraction (Ve) and plasma volume fraction ($V_p$).

MRI results were compared to the histological findings considering the diagnosis of significant PCa based on Gleason score (GS) ≥7 (International Society of Urological Pathology grade group ≥2).

### 2.4. Statistical analysis

Clinical and demographic continuous variables were summarized as median (interquartile range), and categorical data were presented as frequencies and percentages. Differences in the analyzed parameters between benign and malignant groups were calculated using

Mann–Whitney U test or Kruskal–Wallis H test when appropriate. Dependencies between categorical variables were assessed using exact Fisher test.

Interobserver consensus and agreement in measuring $K^{trans}$ and $K_{ep}$ values were evaluated by means of the Spearman and Interclass Correlation Coefficients (ICC).

To measure the overall diagnostic performance and to determine possible cut offs for PK parameters, Receiver Operating Characteristics (ROC) curves were fitted by means of Gaussian kernel estimators with bandwidth selected by unbiased cross validation. As pre-processing, we also dichotomized continuous variables according the "top-left" rule. For clinical purposes, we considered as "clinically acceptable" only cut-off values with an associated accuracy greater of 80%.

Sensitivity, specificity, negative predictive value, positive predictive value and accuracy relative to the pathologic reference standard were calculated by means of Leave One Out Cross Validation (LOOCV) to keep under control too optimistic bias and differences assessed by means of the McNemar test.

Statistical significance was set at $p < 0.05$. P-values were computed by permutation procedures to avoid any distributional assumption. All statistical analyses were performed using SPSS® software package version 20.0 (IBM Corp. Armonk, NY, USA) and R (Foundation for Statistical Computing, Wien, Austria).

## 3. Results

### 3.1. Population and lesions characteristics

Table 2 shows histopathological data and mpMRI findings of the 103 index lesions considered for the analysis. The histological specimens were obtained through prostatectomy (n = 26/103, 25%) or targeted biopsies (n = 77/103; 75%), including MRI-TRUS fusion guided biopsy (n = 69) and MRI-guided in-Bore biopsy (n = 8). Histopathological analysis identified 59/103 (57%) significant PCa (GS ≥ 7): 49/59 (83%) located in the PZ and 10/59 (17%) located in the TZ.

**Table 2**
Clinical, histopathological and radiological characteristic of study cohort (n = 103).

| Parameter | Value |
|---|---|
| **Histological results*** | |
| Benign/normal | 29% (30/103) |
| ASAP/HG-PIN | 7% (7/103) |
| GS 6 | 7% (7/103) |
| GS 7 | 48% (49/103) |
| 3 + 4 | 20% (20/103) |
| 4 + 3 | 28% (29/103) |
| GS 8 | 1% (1/103) |
| GS 9 | 8% (9/103) |
| **Gleason Score*** | |
| GS < 7 | 43% (44/103) |
| GS ≥ 7 | 57% (59/103) |
| **Location at MRI*** | |
| PZ | 82% (84/103) |
| TZ | 18% (19/103) |
| **PI-RADS*** | |
| 2 | 8% (8/103) |
| 3 | 22% (23/103) |
| 4 | 55% (57/103) |
| 5 | 15% (15/103) |
| **PI-RADS 2 vs 3-4-5*** | |
| 2 | 8% (8/103) |
| 3-4-5 | 92% (95/103) |
| **ADC** ($mm^2$/sec)† | 0.74 (0.6-0.9) |
| GS < 7 | 0.9 (0.7-1) |
| GS ≥ 7 | 0.7 (0.6-0.8) |
| **Lesion volume** (cc) † | 0.4 (0.2-0.9) |

Note-PSA = Prostate specific antigen; GS = Gleason score; ADC = Apparent Diffusion Coefficient; PI-RADS = Prostate Imaging Reporting and Data System.
*Data are shown as number of lesions (percentages of total number of lesions).
† Data are reported as median (interquartile range).

**Table 3**
Diagnostic performance of detection GS ≥ 7 cancer at PI-RADS category ≥ 3 for overall, peripheral and transition zone.

| | Overall (n = 103) | PZ (n = 84) | TZ (n = 19) |
|---|---|---|---|
| *Sensitivity* | 98 (58/59) | 98 (48/49) | 100 (10/10) |
| *Specificity* | 16 (7/44) | 14 (5/35) | 22 (2/9) |
| *PPV* | 61 (58/95) | 62 (48/78) | 58 (10/17) |
| *NPV* | 87 (7/8) | 83 (5/6) | 100 (2/2) |
| *Accuracy* | 63 (65/103) | 63 (53/84) | 63 (12/19) |

*Note*-PZ = peripheral zone; TZ = transition zone; PPV = positive predictive value; NPV = negative predictive value. Data are shown as percentages, in parentheses are numerators and denominators.

### 3.2. Performance of PI-RADS v2

We evaluated the diagnostic performance of mpMRI for the prediction of GS ≥ 7 cancers considering PI-RADS ≥ 3 as positive results. For overall detection of GS ≥ 7, PI-RADS classification had a sensitivity of 98% (58/59) and positive predictive value (PPV) of 61% (58/95), identifying 37 false positives, 7 true negatives, 58 true positives and 1 false negative. Results are shown in Table 3.

### 3.3. Permeability analysis

ROI placement and measurements of $K^{trans}$ and $K_{ep}$ values of index lesions had very good interobserver reproducibility [$K^{trans}$ Spearman rho: 0.943 (95% CI: 0.91-0.96); ICC: 0.936 (95% CI: 0.88-0.96). $K_{ep}$ Spearman rho: 0.825 (95% CI: 0.74-0.87); ICC: 0.879 (95% CI: 0.69-0.90)], therefore the mean values between the two readers were used for the analysis.

Quantitative DCE analysis showed significantly higher $K^{trans}$ values in cancerous tissue (GS ≥ 6) compared to the corresponding normal prostatic tissue, both for cancers located in the peripheral zone [PZ-cancer: $269 \times 10^{-3}$/min (148–393) vs PZ-normal tissue: $58 \times 10^{-3}$/min (38–97), $p < 0.001$] and for cancers located in the transitional zone [TZ-cancer: $269 \times 10^{-3}$/min (142–400) vs TZ-normal tissue: $178 \times 10^{-3}$/min (115–248), $p = 0.001$]. Similar results were obtained comparing cancerous and normal tissue for $K_{ep}$ values [PZ-cancer: $345 \times 10^{-3}$/min (199–542) vs PZ-normal tissue: $224 \times 10^{-3}$/min (107–306), $p < 0.001$; TZ-cancer: $353 \times 10^{-3}$/min (199–558) vs TZ-normal tissue: $154 \times 10^{-3}$/min (41–291), $p = 0.001$].

$K^{trans}$ and $K_{ep}$ values were significantly higher in GS ≥ 7 [$326 \times 10^{-3}$/min (220–444) and $429 \times 10^{-3}$/min (226–675)] compared with GS < 7 lesions [$143 \times 10^{-3}$/min (96–307) and $296 \times 10^{-3}$/min (191–420)] ($p < 0.001$ and $p = 0.01$, respectively). However, a considerable overlap of values was observed between the two groups (Fig. 1).

Otherwise $K^{trans}$ and $K_{ep}$ values did not show a different distribution within different GS groups ($p = 0.83$).

Deriving ROC curves for $K^{trans}$ and $K_{ep}$ for GS ≥ 7 the corresponding AUC were 0.75 and 0.65 respectively for overall lesions, 0.84 and 0.70 for PZ lesions, 0.48 and 0.45 for TZ lesions (Fig. 2).

The overall $K^{trans}$ cut-off was $191 \times 10^{-3}$/min (sensitivity 0.95; specificity 0.61, accuracy 0.81). The same cut-off value was found considering PZ lesions (sensitivity 0.96, specificity 0.74, accuracy 0.87). We didn't find a "clinically acceptable" cut-off value for $K_{ep}$ with an accuracy at least of 0.80 (max accuracy 0.65).

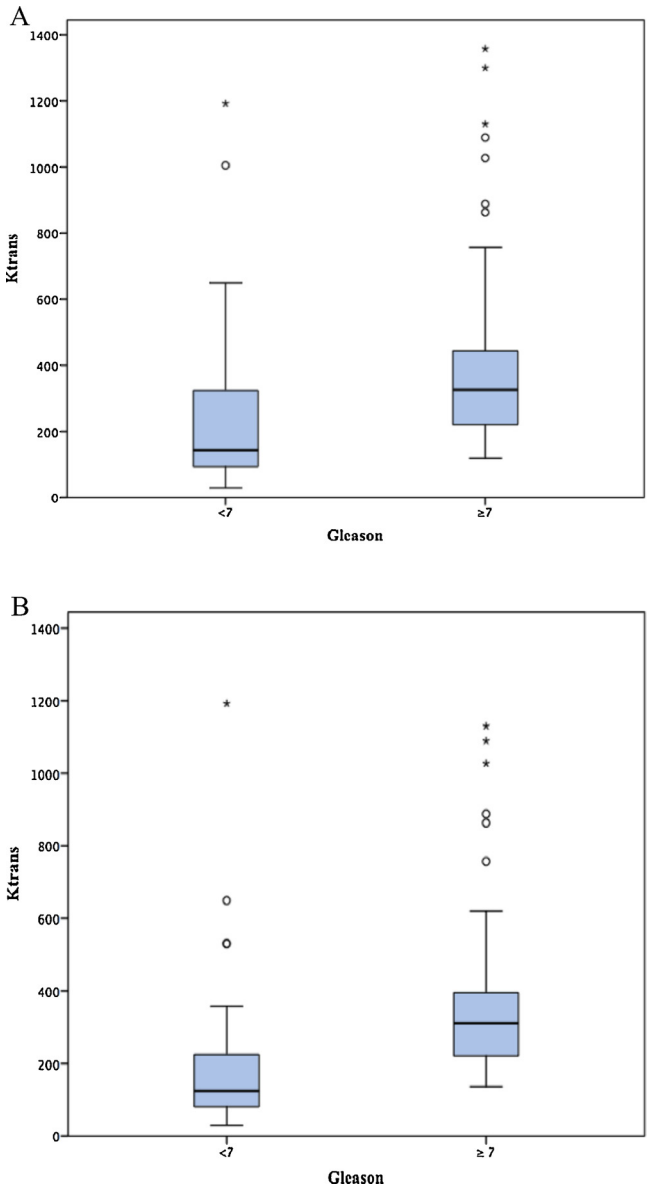


**Fig. 1.** Boxplot showing distribution of $K^{trans}$ according to GS < 7 and ≥7 for overall (a) and PZ lesions (b).

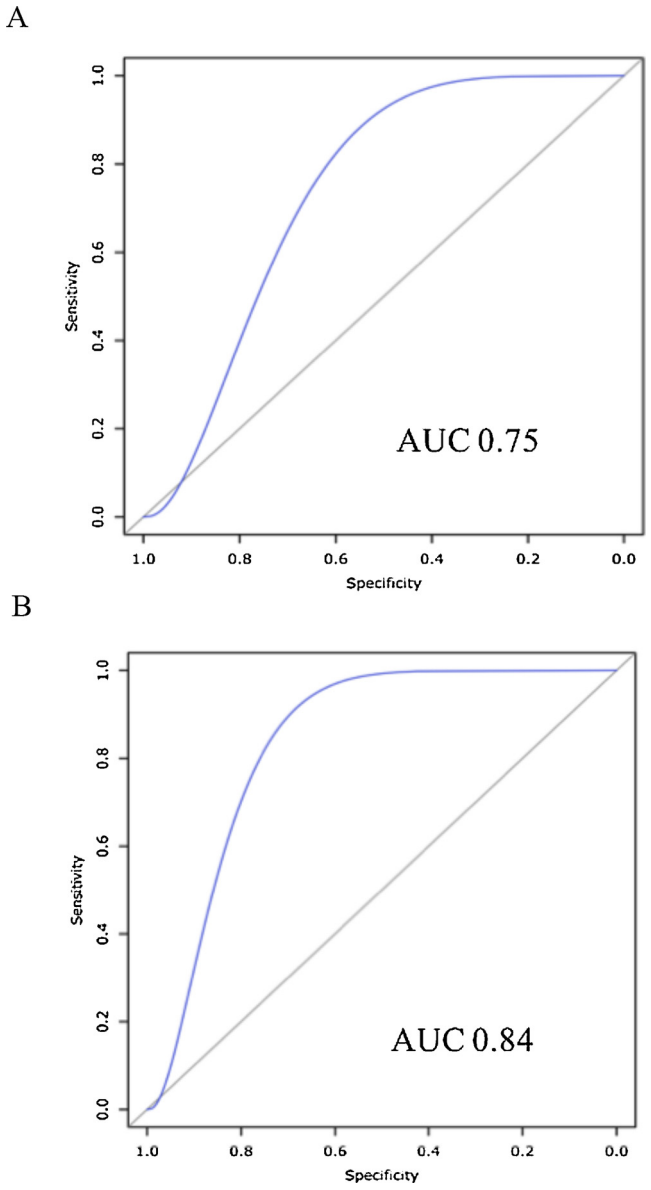


**Fig. 2.** ROC curves and corresponding AUCs for $K^{trans}$ in predicting GS ≥ 7 for overall (a) and PZ (b) lesions.

### 3.4. $K^{trans}$ integration into PI-RADS v2

Positive PI-RADS v2 cases (PIRADS score ≥3) were reclassified as negative when $K^{trans}$ was lower than the cut-off of 191 × $10^{-3}$/min. As result 22 false positives were shifted to true negatives and 3 true positives were reclassified as false negatives. The new diagnostic performance mpMRI for the prediction of GS ≥ 7 considering as positive result PI-RADS≥3 + $K^{trans}$ cut off ≥191 × $10^{-3}$/min is shown in Table 4. The resulting overall PPV and accuracy were 79% (vs 61%) and 82% (vs 63%, p < 0.001) respectively, while sensitivity did not significantly decrease (93% vs 98%, p = 0.25).

Considering only PZ lesions the improvement of diagnostic performance was even more evident: PPV 84% (vs 62%) and accuracy 86% (vs 63%, p < 0.001). An example of a false positive case (PI-RADS 4) of PIRADS v.2 classification, downgraded with the application of $K^{trans}$ cut-off is shown in Fig. 3.

### 3.5. Reclassification of PI-RADS score 3 cases based on $K^{tran}$ cut-off

Out of 103 lesions 23 were classified as PI-RADS 3. Among them, 18 were located in the PZ and 5 in TZ. The histopathological results showed 4 GS ≥ 7 tumors, all located in PZ, and 19 not significant lesions (3 GS = 6 and 16 GS < 6). PI-RADS 3 lesions located in the peripheral zone showed higher $K^{trans}$ value compared to the surrounding normal PZ (median: 296 × $10^{-3}$/min vs 117 × $10^{-3}$/min;

**Table 4**
Diagnostic performance of detection GS ≥ 7 cancer at PI-RADS category ≥ 3 with application of Ktrans cut off of 191 × $10^{-3}$/min for overall, peripheral and transition zone.

| | Overall (n = 103) | PZ (n = 84) | TZ (n = 19) |
|---|---|---|---|
| *Sensitivity* | 93 (55/59) | 94 (46/49) | 90 (9/10) |
| *Specificity* | 66 (29/44) | 74 (26/35) | 33 (3/9) |
| *PPV* | 79 (55/70) | 84 (46/55) | 60 (9/15) |
| *NPV* | 88 (29/33) | 89 (26/29) | 75 (3/4) |
| *Accuracy* | 82 (84/103) | 86 (72/84) | 63 (12/19) |

*Note*-PZ = peripheral zone; TZ = transition zone; PPV = positive predictive value; NPV = negative predictive value. Data are shown as percentages, in parentheses are numerators and denominators.

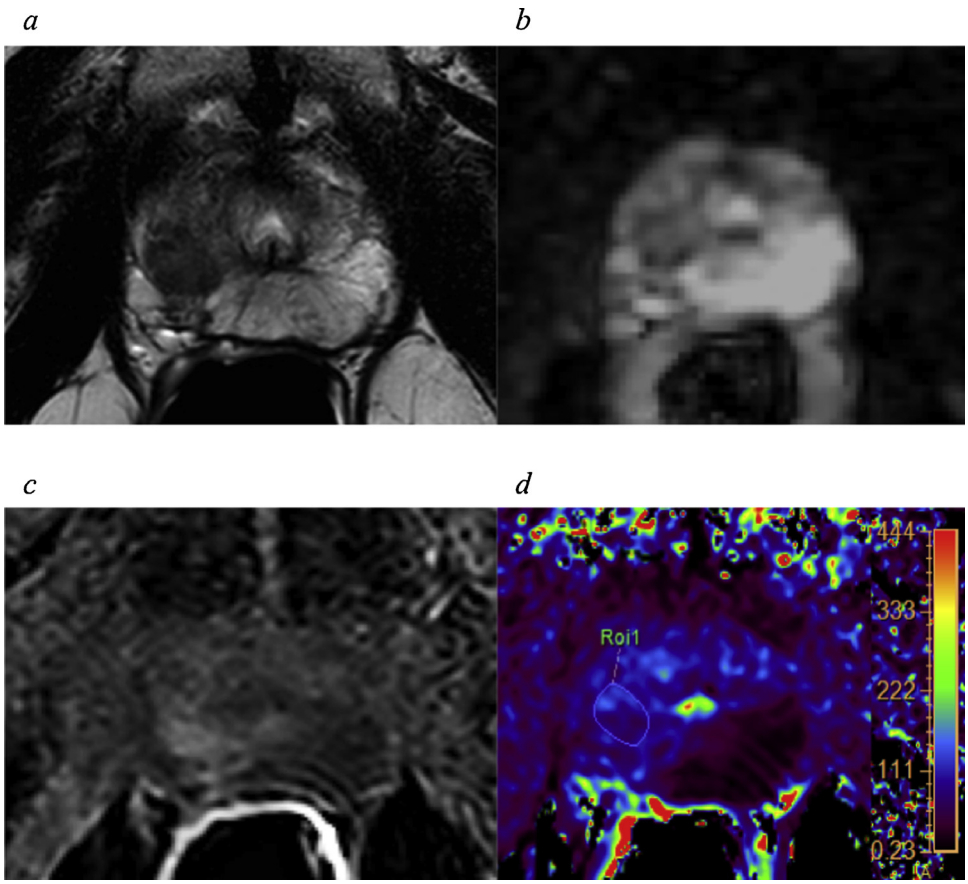


**Fig. 3.** 60 yo man, PSA 6 ng/ml. mpMRI: lesion of apical right peripheral zone with hypointense signal on T2W image (a), low ADC value ($0.98 \times 10^{-3}$ mm$^2$/sec) (b) and iperenhancement on DCE (c) classified as PI-RADS 4. Permeability analysis showed a $K^{trans} = 92 \times 10^{-3}$/min (d). Targeted biopsy was performed confirming absence of pathological tissue.

mean: $428 \times 10^{-3}$/min vs $70 \times 10^{-3}$/min; p = 0.025), while PI-RADS 3 of transition zone did not show any significant difference in PK parameters compared to the normal TZ. Classifying PI-RADS 3 lesions of PZ according to $K^{trans}$ cut-off of $191 \times 10^{-3}$/min value we identified 12 true negatives, 0 false negatives, 2 false positives and 4 true positive (Fisher exact Test p = 0.037). The resulting diagnostic performance was as follows: sensitivity 100%, specificity 86%, PPV 66%, NPV 100%, accuracy 89%.

## 4. Discussion

MpMRI is known to have a remarkable high negative predictive value for detecting significant PCa. This characteristic has led to an increasingly use of this technique as a triage test before prostate biopsy. However, its positive predictive value is relatively low, ranging from 68% down to 20%, depending on the reference test used, the patient population examined and the definition of a positive MRI [8,9,15]. Consequently, the number of avoidable biopsies remains high [22,23].

The recently released PI-RADS v2 guidelines provides a 5-point scale classification that seeks to maintain a balance between achieving high sensitivity for significant disease and avoiding an excessive number of unnecessary biopsies. In our study, we confirmed the high sensitivity (98%) and NPV (87%) of PI-RADS v2 classification, with a still non satisfying specificity (16%) and PPV (61%). Such low value of specificity could be partially explained by the modality of patients' enrollment. Since we retrospectively select men with available histopathological sampling (therefore high risk), we observed a very small number of true negative cases (n = 7). Nevertheless, our data are in line with a recent study published by Simmons et al. [24]. Moreover, including PI-RADS 3 lesions in MRI positive results, although PI-RADS 3 is defined as intermediate risk, we recorded a significant number of false positives (n = 37); but, since we were evaluating mpMRI in the setting of pre-biopsies assessment, the sensitivity (minimizing missing significant PCa) took precedence over specificity and PPV.

Since qualitative analysis of DCE is already included in PI-RADS v2 criteria, we attempt to evaluate if quantitative assessment of permeability parameters may improve MRI diagnostic performance, seeking to increase PPV.

In our study $K^{trans}$ and $K_{ep}$ were significantly higher in cancerous tissue compared to normal prostatic tissue and in significant prostate tumor (GS ≥ 7) compared to nonsignificant lesions (including GS 6, precancerous and benign alteration), as previously reported [25–27]. Consistently with some previous studies we did not observe a significant difference in $K^{trans}$ and $K_{ep}$ values among GS 7, GS 8 and GS 9 [28]. Nevertheless, these results could be influenced by the great numeric difference among our GS classes, with GS 7 representing 74% of all neoplastic findings.

Cho E et al. [25] and Sanz-requena R et al. [27] in their studies proposed a $K^{trans}$ cut-off value for the prediction of significant PCa ($184 \times 10^{-3}$/min and $210 \times 10^{-3}$/min, respectively); these results are highly comparable with our findings ($K^{trans}$ cut-off: $191 \times 10^{-3}$/min).

In our study we were unable to find a satisfying cut-off for $K_{ep}$ values. One possible explanation can be identified in the limited duration of our dynamic study, that sometimes could have terminated before the complete manifestation of the extravascular extracellular space–blood plasma transference phenomenon.

In their recent study Rosenkrantz A et al tested the diagnostic performance of PI-RADS v2 decision rules and proposed different possible adjustments, underling the fact that this classification needs to be improved [29]. To the best of our knowledge our study represents the first attempt to apply quantitative results derived from DCE-MRI analysis to PI-RADS v2 classification, in order to reduce the amount of false positives, increase positive predictive value and therefore limit the number of avoidable biopsies.

The application of $K^{trans}$ cut-off on PI-RADS v2 positive cases (PI-RADS ≥ 3), considering both PZ and TZ lesions, raised PPV from 61% to 79% with a comparable sensitivity (98% vs 93%, p = 0.25). Of note, the 3 false negative results, introduced by the cut-off application, were all GS 3 + 4 lesions with a tumor volume below the significance threshold of 0.5 cc, as reported in PIRADS v2. Splitting PZ from TZ lesions the results were even more promising for PZ (PPV 84% vs 62%), but less satisfying for TZ (PPV 60% vs 58%). These results can be explained by heterogeneous nature of TZ, where benign prostate hyperplasia nodules show avid contrast enhancement similar or even greater, compared to PCa. Moreover, the microvasculature of TZ tumors have been demonstrated to be more heterogeneous compared to PZ tumor, with a larger number of relatively hypovascular lesions, therefore the discriminant value of DCE imaging for TZ PCa remains a conflicting matter [30,31].

The management of intermediate risk lesions (PI-RADS 3) represents a remarkable issue in the clinical setting, with both biopsy and wait-and-see strategies considered as reasonable approach [32]. Appling our $K^{trans}$ cut-off on the PI-RADS 3 lesions of the PZ (n = 18), we correctly identified 12 true negatives and none false negatives, with only 2 false positives (sensitivity 100% and specificity 86%). This finding suggests that $K^{trans}$ cut-off could help in reclassifying PI-RADS 3 in lower or higher risk classes.

Our study has some limitations. Most important, this is a retrospective study that included a selected high-risk population, with small number of true negatives. Furthermore, the histopathological gold standard was obtained in different ways, through radical prostatectomy approximately in a quarter of the patients and through targeted biopsies in the remaining. Another limitation of the study is related to the modality of perfusion images analysis. We used a 'ROI-averaged' analysis that, compared to a 'pixel by pixel analysis', does not consider the spatially heterogeneous enhancement within the ROI. In previous studies and in other oncological setting, some authors suggested that 'pixel by pixel' analysis should be preferred especially to monitor perfusion parameters changes during therapy [33–35]. This seems to be more suitable to capture tumor response, known to be heterogeneous due to different grades of tumor necrosis. In our study the majority of lesions had a small volume (median 0.4 cc; interquartile range 0.2-0.9) and thus the heterogeneity within the lesion is expected to be less relevant. Also, "ROI-averaged analysis" is more commonly used in daily clinical practice compared to "pixel-by-pixel" and therefore it may provide, at the present time, more widely applicable results. Further comparative studies are needed to evaluate the potential impact of these two different methodological approaches on the perfusion analysis results concerning prostate neoplastic lesions.

Lastly, the quantitative approach was not performed using an individualized AIF but through a population based AIF, that is considered justified in clinical setting [36,37] and has been used in previous studies [38,39]. Moreover, PK parameters quantification depends on several factors, such as MRI scanner, DCE-protocols, pharmacokinetic models and permeability analysis software employed. Therefore, it is still not possible to identify a universal cut-off value for $K^{trans}$ for all different clinical settings and every center should establish its own reliable cut-off.

## 5. Conclusions

In conclusion DCE-MRI pharmacokinetic parameters, especially $K^{trans}$, may improve PI-RADS v2 diagnostic performance and its capability in prostate lesions' characterization, decreasing the number of false positive results. Moreover, $K^{trans}$ may optimize the classification of intermediate risk lesions that still represent a clinical management challenge.

## Funding statement

This research did not receive any specific grant from funding agencies in the public, commercial, or not-for-profit sectors.

## References

[1] A. Jemal, M.M. Center, C. DeSantis, E.M. Ward, Global patterns of cancer incidence and mortality rates and trends, Cancer Epidemiol. Biomarkers Prev. 19 (8) (2010) 1893–1907.
[2] L. Li, L. Wang, Z. Feng, Z. Hu, G. Wang, X. Yuan, H. Wang, D. Hu, Prostate cancer magnetic resonance imaging (MRI): multidisciplinary standpoint, Quant. Imaging Med. Surg. 3 (2) (2013) 100–112.
[3] J.C. Weinreb, J.O. Barentsz, P.L. Choyke, F. Cornud, M.A. Haider, K.J. Macura, D. Margolis, M.D. Schnall, F. Shtern, C.M. Tempany, H.C. Thoeny, S. Verma, PI-RADS prostate imaging - reporting and data system: 2015, version 2, Eur. Urol. 69 (1) (2016) 16–40.
[4] L.M. Johnson, B. Turkbey, W.D. Figg, P.L. Choyke, Multiparametric MRI in prostate cancer management, Nat. Rev. Clin. Oncol. 11 (6) (2014) 346–353.
[5] M. Valerio, S. Willis, J. van der Meulen, M. Emberton, H.U. Ahmed, Methodological considerations in assessing the utility of imaging in early prostate cancer, Curr. Opin. Urol. 25 (6) (2015) 536–542.
[6] P.M. Bossuyt, L. Irwig, J. Craig, P. Glasziou, Comparative accuracy: assessing new tests against existing diagnostic pathways, BMJ 332 (7549) (2006) 1089–1092.
[7] L. Schimmoller, M. Quentin, C. Arsov, A. Hiester, P. Kropil, R. Rabenalt, P. Albers, G. Antoch, D. Blondin, Predictive power of the ESUR scoring system for prostate cancer diagnosis verified with targeted MR-guided in-bore biopsy, Eur. J. Radiol. 83 (12) (2014) 2103–2108.
[8] H.U. Ahmed, A. El-Shater Bosaily, L.C. Brown, R. Gabe, R. Kaplan, M.K. Parmar, Y. Collaco-Moraes, K. Ward, R.G. Hindley, A. Freeman, A.P. Kirkham, R. Oldroyd, C. Parker, M. Emberton, P.s. group, Diagnostic accuracy of multi-parametric MRI and TRUS biopsy in prostate cancer (PROMIS): a paired validating confirmatory study, Lancet 389 (10071) (2017) 815–822.
[9] P.C. Moldovan, T. Van den Broeck, R. Sylvester, L. Marconi, J. Bellmunt, R.C.N. van den Bergh, M. Bolla, E. Briers, M.G. Cumberbatch, N. Fossati, T. Gross, A.M. Henry, S. Joniau, T.H. van der Kwast, V.B. Matveev, H.G. van der Poel, M. De Santis, I.G. Schoots, T. Wiegel, C.Y. Yuan, P. Cornford, N. Mottet, T.B. Lam, O. Rouviere, What is the negative predictive value of multiparametric magnetic resonance imaging in excluding prostate cancer at biopsy? A systematic review and meta-analysis from the european association of urology prostate cancer guidelines panel, Eur. Urol. 72 (2) (2017) 250–266.
[10] M. de Rooij, E.H. Hamoen, J.J. Futterer, J.O. Barentsz, M.M. Rovers, Accuracy of multiparametric MRI for prostate cancer detection: a meta-analysis, AJR Am. J. Roentgenol. 202 (2) (2014) 343–351.
[11] J.O. Barentsz, J. Richenberg, R. Clements, P. Choyke, S. Verma, G. Villeirs, O. Rouviere, V. Logager, J.J. Futterer, R. European Society of Urogenital, ESUR prostate MR guidelines 2012, Eur. Radiol. 22 (4) (2012) 746–757.
[12] S.A. Bigler, R.E. Deering, M.K. Brawer, Comparison of microscopic vascularity in benign and malignant prostate tissue, Hum. Pathol. 24 (2) (1993) 220–226.
[13] J.A. Siegal, E. Yu, M.K. Brawer, Topography of neovascularity in human prostate carcinoma, Cancer 75 (10) (1995) 2545–2551.
[14] S. Verma, B. Turkbey, N. Muradyan, A. Rajesh, F. Cornud, M.A. Haider, P.L. Choyke, M. Harisinghani, Overview of dynamic contrast-enhanced MRI in prostate cancer diagnosis and management, AJR Am. J. Roentgenol. 198 (6) (2012) 1277–1288.
[15] J.J. Futterer, S.W. Heijmink, T.W. Scheenen, J. Veltman, H.J. Huisman, P. Vos, C.A. Hulsbergen-Van de Kaa, J.A. Witjes, P.F. Krabbe, A. Heerschap, J.O. Barentsz, Prostate cancer localization with dynamic contrast-enhanced MR imaging and proton MR spectroscopic imaging, Radiology 241 (2) (2006) 449–458.
[16] D. Bonekamp, M.A. Jacobs, R. El-Khouli, D. Stoianovici, K.J. Macura, Advancements in MR imaging of the prostate: from diagnosis to interventions, Radiographics 31 (3) (2011) 677–703.
[17] F. Steinkohl, L. Gruber, J. Bektic, U. Nagele, F. Aigner, T.R.W. Herrmann, M. Rieger, D. Junker, Retrospective analysis of the development of PIRADS 3 lesions over time: when is a follow-up MRI reasonable? World J. Urol. (2017).
[18] J.R. Srigley, P.A. Humphrey, M.B. Amin, S.S. Chang, L. Egevad, J.I. Epstein, D.J. Grignon, J.M. McKiernan, R. Montironi, A.A. Renshaw, V.E. Reuter, T.M. Wheeler, C.o.A.P. Members of the Cancer Committee, Protocol for the examination of specimens from patients with carcinoma of the prostate gland, Arch. Pathol. Lab. Med. 133 (10) (2009) 1568–1576.
[19] P.S. Tofts, Modeling tracer kinetics in dynamic Gd-DTPA MR imaging, J. Magn. Reson. Imaging 7 (1) (1997) 91–101.
[20] H.J. Weinmann, M. Laniado, W. Mutzel, Pharmacokinetics of GdDTPA/dimeglumine after intravenous injection into healthy volunteers, Physiol. Chem. Phys. Med. NMR 16 (2) (1984) 167–172.
[21] G.J. Parker, C. Roberts, A. Macdonald, G.A. Buonaccorsi, S. Cheung, D.L. Buckley, A. Jackson, Y. Watson, K. Davies, G.C. Jayson, Experimentally-derived functional form for a population-averaged high-temporal-resolution arterial input function for dynamic contrast-enhanced MRI, Magn. Reson. Med. 56 (5) (2006) 993–1000.
[22] J.E. Thompson, D. Moses, R. Shnier, P. Brenner, W. Delprado, L. Ponsky, M. Pulbrook, M. Bohm, A.M. Haynes, A. Hayen, P.D. Stricker, Multiparametric magnetic resonance imaging guided diagnostic biopsy detects significant prostate cancer and could reduce unnecessary biopsies and over detection: a prospective study, J. Urol. 192 (1) (2014) 67–74.

[23] J.E. Thompson, P.J. van Leeuwen, D. Moses, R. Shnier, P. Brenner, W. Delprado, M. Pulbrook, M. Bohm, A.M. Haynes, A. Hayen, P.D. Stricker, The diagnostic performance of multi + parametric magnetic resonance imaging to detect significant prostate cancer, J. Urol. 195 (5) (2016) 1428–1435.
[24] L.A.M. Simmons, A. Kanthabalan, M. Arya, T. Briggs, D. Barratt, S.C. Charman, A. Freeman, J. Gelister, D. Hawkes, Y. Hu, C. Jameson, N. McCartan, C.M. Moore, S. Punwani, N. Ramachandran, J. van der Meulen, M. Emberton, H.U. Ahmed, The PICTURE study: diagnostic accuracy of multiparametric MRI in men requiring a repeat prostate biopsy, Br. J. Cancer 116 (9) (2017) 1159–1165.
[25] E. Cho, D.J. Chung, D.M. Yeo, D. Sohn, Y. Son, T. Kim, S.T. Hahn, Optimal cut-off value of perfusion parameters for diagnosing prostate cancer and for assessing aggressiveness associated with Gleason score, Clin. Imaging 39 (5) (2015) 834–840.
[26] P. Gao, C. Shi, L. Zhao, Q. Zhou, L. Luo, Differential diagnosis of prostate cancer and noncancerous tissue in the peripheral zone and central gland using the quantitative parameters of DCE-MRI: a meta-analysis, Medicine (Baltimore) 95 (52) (2016) e5715.
[27] R. Sanz-Requena, L. Marti-Bonmati, R. Perez-Martinez, G. Garcia-Marti, Dynamic contrast-enhanced case-control analysis in 3T MRI of prostate cancer can help to characterize tumor aggressiveness, Eur. J. Radiol. 85 (11) (2016) 2119–2126.
[28] A.R. Padhani, C.J. Gapinski, D.A. Macvicar, G.J. Parker, J. Suckling, P.B. Revell, M.O. Leach, D.P. Dearnaley, J.E. Husband, Dynamic contrast enhanced MRI of prostate cancer: correlation with morphology and tumour stage, histological grade and PSA, Clin. Radiol. 55 (2) (2000) 99–109.
[29] A.B. Rosenkrantz, J.S. Babb, S.S. Taneja, J.M. Ream, Proposed adjustments to PI-RADS version 2 decision rules: impact on prostate cancer detection, Radiology 283 (1) (2017) 119–129.
[30] C.G. van Niekerk, J.A. Witjes, J.O. Barentsz, J.A. van der Laak, C.A. Hulsbergen-van de Kaa, Microvascularity in transition zone prostate tumors resembles normal prostatic tissue, Prostate 73 (5) (2013) 467–475.
[31] A.L. Chesnais, E. Niaf, F. Bratan, F. Mege-Lechevallier, S. Roche, M. Rabilloud, M. Colombel, O. Rouviere, Differentiation of transitional zone prostate cancer from benign hyperplasia nodules: evaluation of discriminant criteria at multiparametric MRI, Clin. Radiol. 68 (6) (2013) e323–30.
[32] H. Liddell, R. Jyoti, H.Z. Haxhimolla, Mp-MRI prostate characterised PIRADS 3 lesions are associated with a low risk of clinically significant prostate cancer - a retrospective review of 92 biopsied PIRADS 3 lesions, Curr. Urol. 8 (2) (2015) 96–100.
[33] S.J. Ahn, C.S. An, W.S. Koom, H.T. Song, J.S. Suh, Correlations of 3T DCE-MRI quantitative parameters with microvessel density in a human-colorectal-cancer xenograft mouse model, Korean J. Radiol. 12 (6) (2011) 722–730.
[34] D. He, M. Zamora, A. Oto, G.S. Karczmar, X. Fan, Comparison of region-of-interest-averaged and pixel-averaged analysis of DCE-MRI data based on simulations and pre-clinical experiments, Phys. Med. Biol. 62 (18) (2017) N445–N459.
[35] C.R. Haney, X. Fan, E. Markiewicz, D. Mustafi, G.S. Karczmar, W.M. Stadler, Monitoring anti-angiogenic therapy in colorectal cancer murine model using dynamic contrast-enhanced MRI: comparing pixel-by-pixel with region of interest analysis, Technol. Cancer Res. Treat. 12 (1) (2013) 71–78.
[36] T. Franiel, B. Hamm, H. Hricak, Dynamic contrast-enhanced magnetic resonance imaging and pharmacokinetic models in prostate cancer, Eur. Radiol. 21 (3) (2011) 616–626.
[37] M. Azahaf, M. Haberley, N. Betrouni, O. Ernst, H. Behal, A. Duhamel, A. Ouzzane, P. Puech, Impact of arterial input function selection on the accuracy of dynamic contrast-enhanced MRI quantitative analysis for the diagnosis of clinically significant prostate cancer, J. Magn. Reson. Imaging 43 (3) (2016) 737–749.
[38] D.L. Langer, T.H. van der Kwast, A.J. Evans, J. Trachtenberg, B.C. Wilson, M.A. Haider, Prostate cancer detection with multi-parametric MRI: logistic regression analysis of quantitative T2, diffusion-weighted imaging, and dynamic contrast-enhanced MRI, J. Magn. Reson. Imaging 30 (2) (2009) 327–334.
[39] A. Oto, C. Yang, A. Kayhan, M. Tretiakova, T. Antic, C. Schmid-Tannwald, S. Eggener, G.S. Karczmar, W.M. Stadler, Diffusion-weighted and dynamic contrast-enhanced MRI of prostate cancer: correlation of quantitative MR parameters with Gleason score and tumor angiogenesis, AJR Am. J. Roentgenol. 197 (6) (2011) 1382–1390.